Vertical variation of turbulent entrainment mixing processes in marine stratocumulus clouds using high resolution digital holography

Neel Desai[1], Yangang Liu[1], Susanne Glienke[2], Raymond A. Shaw[3], Chunsong Lu[4], Jian Wang[1,5]and Sinan Gao[4]

[1]Environmental and Climate Sciences Department, Brookhaven National Laboratory, Upton, NY
[2]Atmospheric Sciences and Global Change Division, Pacific Northwest National Laboratory, Richland WA
[3]Atmospheric Sciences Program, Department of Physics, Michigan Technological University, Houghton, MI
[4]Collaborative Innovation Center on Forecast and Evaluation of Meteorological Disasters, Key Laboratory for Aerosol Cloud Precipitation of China Meteorological Administration, Nanjing University of Information Science and Technology, Nanjing, China
[5]Center for Aerosol Science and Engineering, Department of Energy, Environmental and Chemical Engineering, University of Washington, St. Louis, MO

Key Points:

- High resolution airborne holographic measurements show that entrainment mixing behavior changes from inhomogeneous near cloud top to homogeneous near cloud base for marine stratocumulus clouds.
- Vertical variation of entrained air relative humidity plays an important role in determining the entrainment mixing behavior and a model is proposed to consider it.
- Vertical variation of entrainment-mixing behavior can be explained by covariations of turbulence and microphysics when the modified droplet evaporation time is used.

Corresponding author: Neel Desai, desai@bnl.gov

Abstract

Marine stratocumulus clouds contribute significantly to the Earth's radiation budget due to their extensive coverage and high albedo. Yet, subgrid variability in cloud properties such as aerosol concentration, droplet number and precipitation rates lead to considerable errors in global climate models. While these clouds usually have small vertical extent, turbulent entrainment-mixing and precipitation can generate significant variations in droplet number, size and relative dispersion with altitude. In this paper, we analyze turbulent entrainment-mixing processes and the variability in cloud microphysical properties as a function of height within a warm marine stratocumulus cloud layer over the Eastern North Atlantic. We use high resolution airborne holographic measurements and compare them with local turbulence measurements. We find that entrainment-mixing is primarily inhomogeneous near cloud top and homogeneous near cloud base. Further analysis of Damköhler number and transition scale number are able to explain the mixing mechanisms at different cloud heights using phase relaxation but not droplet evaporation as the microphysical time scale. A modified droplet evaporation time scale which considers local saturation deficit using a simple linear mixing model is developed and it is able to reliably explain the observed mixing mechanisms. This study reinforces the importance of turbulent mixing and use of appropriate microphysical time scales in determining cloud microphysical processes.

Plain Language Summary

Warm boundary layer clouds over the oceans cover vast extents of the Earth's surface and influence the Earth's temperature considerably. We study these clouds over the Eastern North Atlantic using high resolution holographic measurements which can resolve microphysical features at small scales. We observe variability in cloud microphysical properties with height within these clouds with the largest droplets occurring near cloud top. We also attempt to explain the vertical variation in turbulent entrainment-mixing processes using concurrent turbulence measurements and propose a new microphysical time scale to explain variation in cloud microphysics with height.

1 Introduction

Boundary layer clouds such as stratocumulus clouds cover nearly 20% of Earth's surface (Warren et al., 2007; Eastman et al., 2011). Of these, marine stratocumulus clouds are most abundant especially off the west coast of most continents with coverage in some regions exceeding 60% of the time (Wood, 2012). Marine stratocumulus clouds have relatively high albedo compared to the water surface below and their cloud top temperature is not very different from the water surface temperature due to their low altitude resulting in a significant cooling effect on the Earth's radiative budget (Stephens & Greenwald, 1991). They are maintained by strong cloud top radiative cooling and a continuous supply of moisture from the ocean surface below. However, they are often not uniform and form intricate subgrid scale structures which have been difficult to represent in global climate models (Glassmeier & Feingold, 2017). Observations from tethered balloon measurements of visible and near infrared albedos have indicated that inhomogeneities in cloud structure and drizzle may allow visible light to pass through and affect cloud albedo as well as radiative properties (Duda et al., 1991).

Cloud top entrainment-mixing has long been considered as one of the primary processes causing inhomogeneity in cloud structure by influencing droplet trajectories and supersaturation values, resulting in broad droplet spectra (Cooper, 1989; Brenguier & Grabowski, 1993; Mellado, 2017). Multiple studies have directly attributed cloud droplet spectral broadening and warm rain formation to turbulent entrainment mixing in clouds (Andrejczuk et al., 2006; Liu & Hallett, 1998; Liu & Daum, 2000; Yum & Hudson, 2001). A broad droplet size distribution facilitates warm rain formation by enhancing the collision-

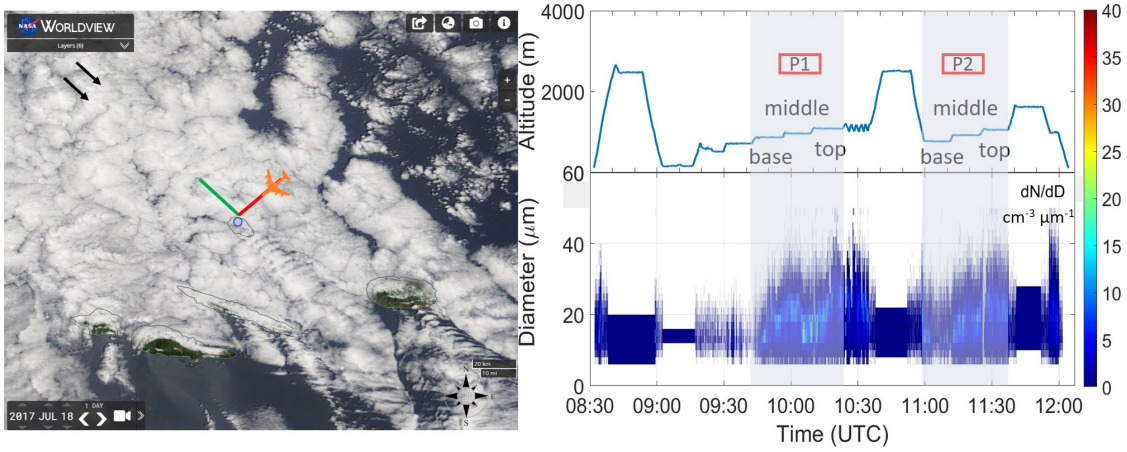

Figure 1. Left panel shows a NASA worldview image of the stratocumulus deck being measured with an L-shaped flight pattern overlayed for RF18 (July 18, 2017). The green and red lines represent flight legs parallel and perpendicular to the mean wind direction (from the northwest as indicated by black arrows) respectively. We shall refer to these flight legs as along-wind and cross-wind respectively. The right panel shows flight altitude, droplet number density and droplet size measured by HOLODEC along the flight path. RF18 consisted of two cloud incursions marked as passes P1 and P2. Each incursion consisted of measurements made at least three altitudes labelled as cloud base, middle and top respectively. Only the along wind legs at each altitude are studied here. The blue dot on the island represents the ARM Eastern North Atlantic field measurement facility.

coalescence process (Lasher-trapp et al., 2005; Cooper et al., 2013). It also facilitates aerosol removal processes within clouds through sedimentation, thus further affecting cloud radiative properties (Hill et al., 2009). Air turbulence likely plays an important role in determining what type of entrainment mixing occurs (Shaw, 2003). If the time required for turbulent mixing of dry air and cloudy parcels of air is smaller than the time required for the droplets to completely evaporate, a majority of the droplets will experience the reduction in supersaturation. This will lead to a reduction in size for most droplets and is called Homogeneous Mixing (HM) (Warner, 1973). However, if the mixing time scale is larger than the droplet reaction time, some droplets will completely evaporate and replenish the decrease in water vapor before other droplets can feel the reduction in supersaturation. This leads to the mean volume radius remaining unchanged but a reduction in droplet number concentration and is called Inhomogeneous Mixing (IM) (Baker et al., 1980). IM decreases the droplet number and thus can allow droplet growth and promote drizzle formation through collision coalescence (CC) (Magaritz-Ronen et al., 2016; Hoffmann & Feingold, 2019). However, entrainment-mixing processes in ambient clouds often fall between the two extremes, and remain quite controversial. For example, Lu et al. (2011) found the dominance of IM over HM while analyzing continental stratocumulus clouds sampled over the U.S. Department of Energy's (DOE) Atmospheric Radiation Measurement (ARM) Southern Great Plains site. At the same time, Yeom et al. (2017) also studied continental stratocumulus clouds collected over the same site but during the Routine ARM Aerial Facility (AAF) Cloud with Low Optical Water Depths (CLOWD) Optical Radiative Observations (RACORO) campaign and found primarily HM occurring due to dryer environmental conditions.

Even more poorly studied and elusive are the vertical variations of entrainment-mixing behavior with height above cloud base. Yum et al. (2015) argue that for marine

stratocumulus, mixing can be inhomogeneous near cloud top and homogeneous near cloud base. This occurs due to negative buoyancy of entrained cloud top parcels resulting in vertical circulation within the cloud deck (Telford & Chai, 1980; J. Wang et al., 2009). This vertical circulation adds to spatial inhomogeneity within the cloud as a function of altitude which should promote droplet growth near cloud top and drizzle formation in marine stratocumulus clouds. However, using a traditional droplet measurement technique, Yum et al. (2015) could not observe such a variation in mixing type with height and implored further research to validate their inferences using higher resolution droplet measurements. Furthermore, all these processes are affected by small scale turbulence with length scales of the order of centimeters (Beals et al., 2015). Prior studies have shown that the apparent entrainment-mixing processes are scale dependent and that observed entrainment mixing type may change with averaging scale (Lu et al., 2014; S. Gao et al., 2020). Traditional droplet measurement techniques suffer from sampling artifacts which can distort mixing signatures due to drop by drop detection techniques (Burnet & Brenguier, 2007). However, studies of entrainment-mixing using local (non-spatially averaged) microphysical properties at the centimeter scale are extremely rare due to limited measurements.

In this paper, we use high resolution holography to provide local centimeter scale measurements of cloud droplet size distributions and number concentrations. This avoids the effects of averaging across meter scale regions which may be affected by varying degrees of mixing. Using these high resolution droplet measurements, we study entrainment-mixing and droplet growth mechanisms in marine stratocumulus clouds with respect to altitude and turbulence parameters. We want to know if we can conclusively observe the different mixing behaviors at different altitudes within a cloud as suggested by Yum et al. (2015). If the mixing types are different at various altitudes, how does the height dependence affect droplet size and drizzle formation? Also, why are the mixing types different and can we explain their vertical variation using dynamical measures? The paper proceeds as follows: in section 2, we describe the atmospheric conditions prevalent during the measurements and the instrumentation that was used. In section 3 we present observational results and discuss the findings. In section 4 we propose a new vertical mixing model for entrained air subsaturation and in section 5, we interpret the results from the new model in order to obtain a better understanding of cloud microphysics. Finally in section 6, we summarize our findings and discuss possible implications for the microphysics community when considering different microphysical timescales for entrainment-mixing processes.

2 Measurements

The measurements used in this study were taken during the Intensive Observation Periods (IOPs) of the DOE Aerosol and Cloud Experiments in the Eastern North Atlantic (ACE-ENA) campaign. The field campaign consisted of 20 Research Flights (RF) during June-July 2017 (IOP1) and 19 research flights during January-February 2018 (IOP2) using the ARM Aerial Facility (AAF) Gulfstream-1 (G-1) aircraft (J. Wang et al., 2019). However, hologram data reconstruction is computationally expensive and only a handful of flights have been reconstructed and analyzed to date. For this study, we use data from RF18 IOP1, on July 18, 2017 since this flight sampled a homogeneous stratocumulus cloud layer with aircraft penetrations at multiple altitudes. Fig. 1 shows a satellite view of the stratocumulus cloud deck and a flight altitude pattern for RF18. The flight pattern at each altitude was L-shaped with one along-wind and one cross-wind leg. The aircraft would then ascend to a higher altitude and repeat the same L-shaped pattern again. In this study, we focus on the along-wind legs at each altitude with primarily head winds along the flight path. As can be seen, two cloud passes P1 and P2 were conducted over the same location, just north of the island of Graciosa, Portugal. Each cloud pass consisted of at least three cloud penetrations at different altitudes, named cloud base,

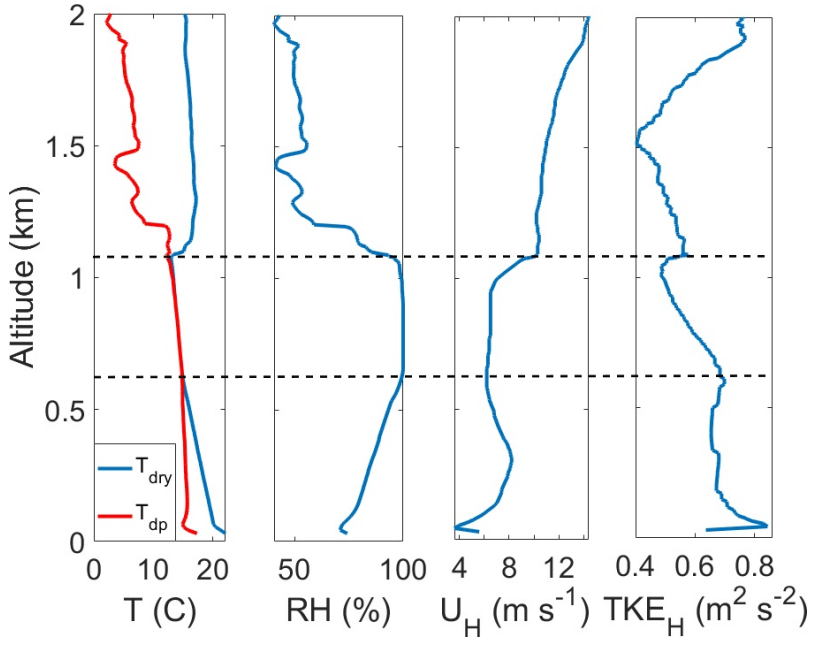

Figure 2. Balloon borne sounding (SONDE) measurements taken over the ENA field measurement site at 1138 UTC on July 18, 2017 show the thermodynamic conditions close to the measurement region. From left to right, are dry (T_{dry}) and dew point temperature (T_{dp}), relative humidity (RH), horizontal wind speed and horizontal turbulence kinetic energy (TKE_H). The dotted lines roughly border the region where RH reaches 100 % and can be expected to be the cloud layer.

middle and top respectively. Note that this naming system is relative and does not indicate that the cloud base leg was truly level with cloud base and likewise with cloud top due to variation in cloud base and top levels respectively. Small cloud segments (1-2 minutes) from these roughly cloud legs are selected for analysis such that the cloud properties (e.g., mean droplet number concentration and mean droplet radius) remain relatively constant along each sampled cloud segment. This is done to ensure temporal and spatial uniformity in cloud properties for the analyzed cloud segments as well as to minimize the effects of cloud base/top height variation. Fig. 2 shows the thermodynamic profiles from a balloon sounding taken on the morning of July 18, 2018 at 11:38 hrs UTC. We can see the presence of a cloud layer between approximately 600 m and 1100 m altitude highlighted by the dotted lines. The sounding was launched from the ARM ENA measurement facility located near the north-western coast of the island whereas the higher elevation regions are located near the southern end of the island. Due to this topographical feature, we can safely assume that the aircraft measurements made upwind of the facility as well as the sounding made from the facility, are measuring the unperturbed marine boundary layer (Giangrande et al., 2019).

For measuring cloud microphysical properties such as droplet size and number concentration, we use the Holographic Detector for Clouds (HOLODEC) which can measure cloud droplets of radii exceeding 3 μm up to mm range (J. P. Fugal et al., 2004; Spuler & Fugal, 2011). HOLODEC provides three dimensional images of a 1 cm^2 x 13 cm volume, thus allowing local centimeter scale measurements of cloud properties such as number concentration and size distribution. Each image or hologram is obtained at 3.3 Hz and for a mean flight speed of 100 m s^{-1}, sampling occurs approximately every 33 m. Thus each 1-2 minute cloud segment generates between 200-300 holograms, each of which

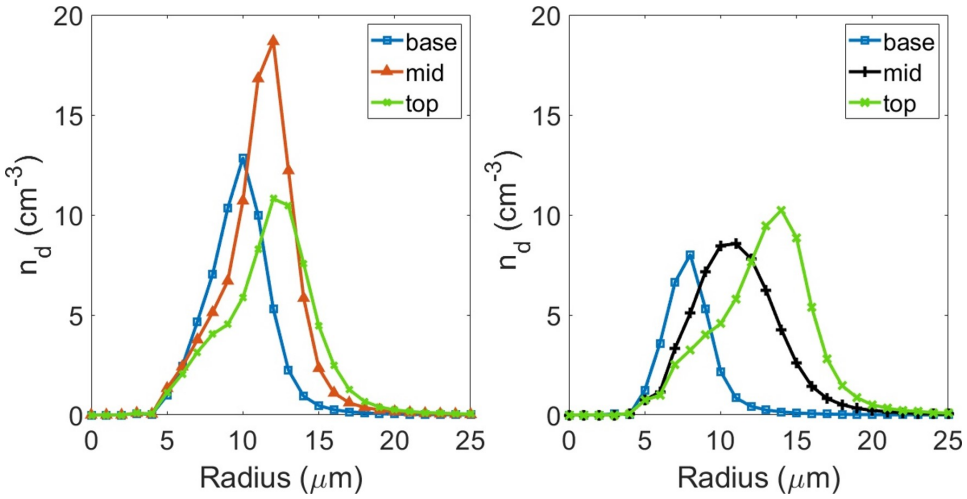

Figure 3. Cloud droplet size distributions for (left) P1 and (right) P2. These indicate that mean size as well as width of the distribution increases with altitude within the cloud. P2 shows a steady shift of the size distribution peak with height, while for P1, the shift is less pronounced.

provides an instantaneous droplet size distribution and number concentration without the need for averaging. The holograms so obtained were digitally reconstructed using high performance computing algorithms to detect potential particles (J. P. Fugal et al., 2009). Droplets were identified from these particles using both supervised and unsupervised machine learning techniques which utilize decision trees for identification as well as a validation and show a 97% accuracy for cloud droplets(Henneberger, 2013). Prior studies have also shown these results to be reliable and comparable to other on-board instruments (J. Fugal & Shaw, 2009; Beals et al., 2015).

For additional data reliability, only droplets with radii larger than 5 μm and number concentrations larger than 10 cm^{-3} were considered. Droplet size distributions obtained using HOLODEC showed good agreement with other instruments on-board the aircraft (SI). For RF18, the along wind flight legs consisted of droplets with radii mostly larger than 5 μm while the cross-wind legs consisted of a large number of droplets smaller than 5 μm (Zhang et al., 2020). Thus, as mentioned earlier, only data from the along-wind legs was considered in this study. The reason for the mismatch in droplet size between two flight legs at the same altitude while interesting, requires a separate investigation and is not considered here. For turbulence measurements, the AIMMS-20 probe is used to collect high resolution wind velocity, altitude, temperature and relative humidity at 20 Hz.

3 Results and analysis

3.1 Size distributions

Fig. 3 shows the droplet size distributions for P1 and P2 at their respective altitudes. For P1, the size distributions at cloud base has a smaller mean radius compared to cloud top with the size distribution at cloud middle lying between these two values. The size distributions for P2 also show similar altitudinal behavior like P1 with different magnitudes however. At cloud base, P2 has a smaller mean radius compared to P1 which could be due to the P2 cloud base flight altitude being not at the same level relative to the cloud base as P1. This is because the sampling altitude for the cloud bases was determined visually by the pilot. P1 and P2 cloud base flight altitude was 872 m

and 775 m above ground respectively, while ground based Ceilometer measurements indicate an average cloud base height of 750 m during the same time period. While the droplet size distribution skewness values are affected by the $5\mu m$ radius cutoff, the skewness ratio of P2 vs P1 cloud base suggests a 27% more positively skewed size distribution for P2 compared to P1.

Along with mean radius, standard deviation in droplet radius also increases with height for both P1 and P2 (table 1) indicating that the size distributions are broader near cloud top compared to cloud base. The increase in standard deviation with height is in contrast with what would be expected from growth by adiabatic condensation. The difference in mean radius with height is more pronounced for P2 compared to P1 while the droplet number concentrations are smaller for P2 compared to P1. The steady increase in droplet properties such as radius and liquid water content (LWC) with height within the cloud layer agrees with previous observations of marine stratocumulus clouds layers by (Duynkerke et al., 1995; Yum & Hudson, 2005; J. Wang et al., 2009). Other properties such as average relative dispersion (d), defined as the ratio of standard deviation to the mean radius for the cloud segment stays relatively constant with height since both radius and standard deviation increase steadily with height. This suggests that instead of average values of d, a per hologram relative dispersion behavior at each altitude may provide a better insight into the underlying microphysics. Droplet number concentration shows an increase with height with cloud base having the lowest value for both P1 and P2. This may occur due to above cloud top aerosol activation or cloud base height variation (J. Wang et al., 2009). Another possibility is an underestimation of the droplet count especially near cloud base where the droplet radii are the smallest due to the 5 μm radius detection limit for HOLODEC. Thus, we can expect a steady increase in the number of droplets detected with height as droplets grow in size as they ascend through the cloud. However, P1 shows a decrease in number concentration from cloud middle towards cloud top which may indicate extensive droplet evaporation near cloud top due to possible entrainment-mixing. We now examine the entrainment-mixing mechanisms along with relative dispersion at each altitude to further understand their effect and microphysical behavior with height.

3.2 Mixing diagram analysis

Mixing diagrams have been widely used to indicate microphysical behavior of droplets during entrainment mixing events in stratocumulus clouds (Paluch & Knight, 1984; Pawlowska & Brenguier, 2000). The X-axis represents the droplet number concentration normalized by the adiabatic value and the Y-axis represents the mean droplet volume normalized by the adiabatic value. In real clouds however, estimating the above mentioned adiabatic values can be difficult, and hence the maximum number concentration is often used as a substitute (Beals et al., 2015). Here, we consider the hologram with the maximum number concentration (n_o) as the least diluted sample for each cloud segment and the corresponding mean volume radius (mvr) as r_0. Fig. 4 shows mixing diagrams from the six cloud segments shown in fig. 3, with each point colored according to the relative dispersion for each hologram. The left panels (**a,d**) show a decrease in mvr with decrease in droplet number concentration which is an indication of HM with data points progressing towards lower liquid water content with dilution. This signature is observed near cloud base for both P1 and P2. The right panels (**c,f**) show a relatively constant mvr with reduction in droplet number concentration which indicates IM. This signature is observed at cloud top for both P1 and P2. The middle panels (**b,e**) display the cloud middle segments during P1 and P2 respectively. Panel **b** shows a signature similar to IM, however some holograms show larger mvr compared to the adiabatic value. This behavior could occur due to a number of potential reasons such as: IM followed by adiabatic growth (IM&G), where a cloud parcel with reduced droplet number concentration due to IM when subjected to the same updraft as the surrounding parcels at the same altitude, may generate super-adiabatic droplets due to larger supersaturation fluctuations (Baker et al., 1980;

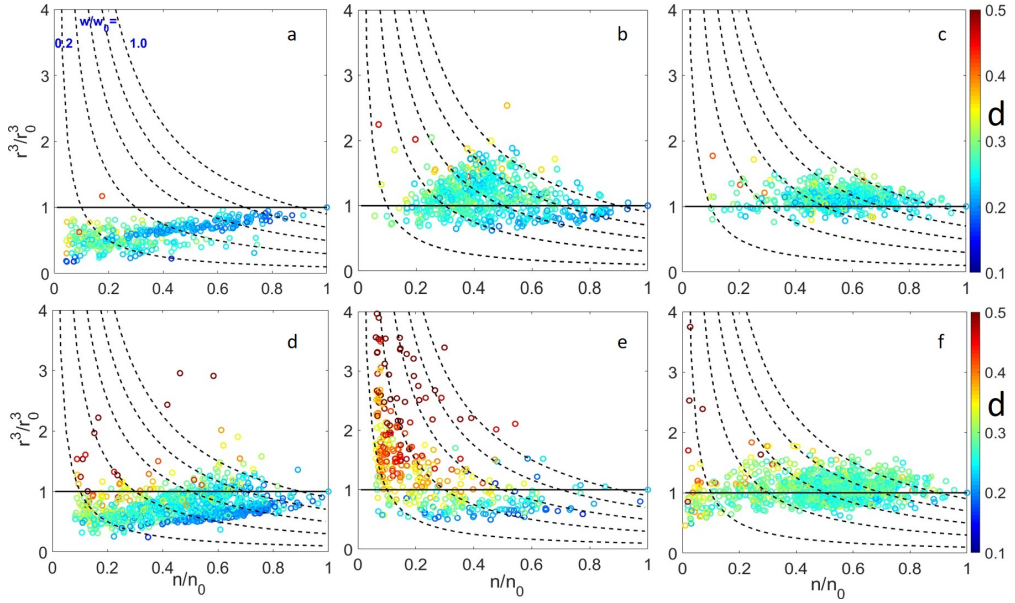

Figure 4. Mixing diagrams with normalized droplet number concentration on the X-axis and normalized droplet volume on the Y-axis. The dotted lines represent constant LWC lines with the ratio of w/w_0 corresponding to the ratio of LWC in the holograms to that of the least diluted sample respectively. Each data point represents the mean droplet volume and number concentration for each hologram during a cloud segment and is colored by the corresponding relative dispersion (d). The top and bottom rows are from P1 and P2 respectively. Left to right columns increase in altitude within the cloud. (a) shows homogeneous mixing (HM) where droplet volume decreases with increasing dilution for P1 cloud base. (b) shows possible signature of inhomogeneous mixing followed by adiabatic growth (IM&G) at P1 cloud middle. (c) shows signatures of inhomogeneous mixing (IM) where mean droplet volume stays constant with volume for P1 cloud top. (d) shows HM at P2 cloud base, (e) shows possible collision-coalescence (CC) at P2 middle and (f) indicates IM at P2 cloud top.

Lasher-trapp et al., 2005; Yang et al., 2016). However artifacts due to measurement uncertainty in LWC values along a cloud segment (Burnet & Brenguier, 2007) or variation in cloud base height (J. Wang et al., 2009) may also lead to data points with super-adiabatic mvr due to an inaccurate estimation of the adiabatic mvr. Panel **e** however, shows considerable increase in mvr at low number concentrations along with a significant increase in relative dispersion as well. Desai et al. (2019) argued that this is a signal for droplet growth via collision-coalescence (CC). This is observed at cloud middle level for P2.

Panels **b**, **e** indicate that the cloud segment sampled during P1 does not contain many large drizzle sized droplets, but the P2 cloud segment does which leads to an interesting observation (SI). Conventionally, larger droplet number concentrations promote collision-coalescence. However recent studies have shown that lower droplet number concentrations can lead to larger droplet sizes and a broadening of the droplet size distribution through turbulent condensational growth (S. Chen, Yau, Bartello, & Xue, 2018; Chandrakar et al., 2016; Sardina et al., 2015; Paoli & Shariff, 2009). Larger droplet sizes and broader size distributions tend to have a much larger effect of cloud auto-conversion rate since the rate is proportional to the 6^{th} power of droplet radius. As can be seen in table 2, mean droplet radii were larger for P2 cloud middle and top segments compared to P1. The width of the distributions were also larger for P2 compared to P1. These fac-

tors can sometimes override the effect of droplet number concentration and promote higher auto-conversion rates. Measured auto-conversion rate value (Liu et al., 2007; Xie & Liu, 2009) for the P2 cloud middle segment was $4e^{-8}$ kg m^{-3} compared to $2e^{-9}$ kg m^{-3} for P1 cloud middle segment. This promotion of warm rain initiation during smaller droplet number concentration values has been observed previously in marine stratocumulus clouds by (Goren & Rosenfeld, 2015; Wood et al., 2018; Desai et al., 2019; Ghate & Cadeddu, 2019). Drizzle initiation during P2 may also explain the steady increase in droplet number concentration with height since drizzle droplets will tend to collect other droplets during sedimentation and reduce droplet concentrations at lower altitudes. It is also interesting to note that TKE dissipation rates for P2 were lower than those for P1 (table 2) indicating weaker turbulence when the CC signature was observed. This goes against the general notion that stronger turbulence should promote droplet collision-coalescence (Shaw, 2003; Grabowski & Wang, 2013). However, recent studies have shown that for broad size distributions subject to sedimentation and low dissipation rates such as those observed in marine stratocumulus clouds, the enhancement effect of turbulence on droplet collisions for broad size distributions is weak (L.-P. Wang & Grabowski, 2009; Woittiez et al., 2009; S. Chen, Yau, & Bartello, 2018). Thus, we still observe CC signature during P2 even though the turbulence was weaker compared to P1 suggesting that turbulence is not playing a major role in drizzle initiation. Lack of a CC signature during P1 resulted in a higher droplet number concentration for P1 cloud middle level compared to P2 cloud middle which was affected by CC. However, this does not mean that there wasn't any drizzle during the P1 time period, since ground based measurements from the ARM research facility on Graciosa suggest a continuous drizzling stratocumulus deck. The above discussion only addresses why we may have observed CC signature during the cloud middle segment during P2 but not during P1.

Relative dispersion behavior for the HM cases at cloud base shows considerable scatter and negative correlations (R-values of -0.50 and -0.45) with droplet number concentration for P1 and P2 respectively. These correlations are statistically significant with p-values of 0.00 and 0.00 respectively, where p-values below 0.05 indicate statistical significance at the 95% significance level (Fisher, 2006). The negative correlation can be observed as an increase in relative dispersion with decreasing droplet number concentration in fig. 4 panels **a**,**d**. This behavior can be attributed to the reduction in droplet size due to entrainment-mixing resulting in smaller droplets and an increase in standard deviation (Hudson & Yum, 1997). Cloud top relative dispersion also shows a negative but not statistically significant (p-value of 0.08) correlation (R-value of -0.16) for P1 and a statistically significant (p-value 0.01) negative correlation (R-value of -0.21) with droplet number concentration for P2. This suggests that the negative correlation of relative dispersion values with droplet number concentration is much weaker near cloud top compared to cloud base as can be seen in fig. 4 panels **c**,**f**. This weaker correlation is expected since IM results in complete evaporation of some cloud droplets while leaving others unaffected. We also observe that holograms with the lowest droplet concentrations that show larger values of relative dispersion also show higher mvr for both P1 and P2 similar to panel **e**. These holograms may show early signs of CC occurring near cloud top, but the small number of holograms which show this behavior makes it difficult to quantify. This is not uncommon since recent studies do suggest that IM near cloud top can create larger supersaturation fluctuations allowing existing droplets to grow larger and form drizzle droplets (Cooper et al., 2013; Yang et al., 2019).

3.3 Homogeneous mixing degree

We now attempt to verify our visual observations of the mixing diagrams by examining the homogeneous mixing degree at each altitude. For the mixing diagrams shown in fig. 4, the homogeneous mixing degree (ψ) can be defined as (Lu et al., 2013) :

Level	$\overline{r}(\mu m)$	$n(cm^{-3})$	$\sigma_r(\mu m)$	d	$LWC(g\ kg^{-1})$	ψ
P1 Base	9.5	60.0	2.2	0.23	0.26	0.28
Mid	11.1	86.7	2.5	0.22	0.58	−0.21
Top	12.2	74.9	3.1	0.26	0.65	−0.04
P2 Base	9.1	48.5	2.4	0.26	0.15	0.25
Mid	11.5	66.5	3.2	0.28	0.42	−0.33
Top	12.9	69.8	3.4	0.26	0.59	−0.01

Table 1. Cloud microphysical properties such as mean radius ($\overline{r}$), mean droplet number concentration (n), standard deviation in radius (σ_r), relative dispersion (d), liquid water content (LWC) and homogeneous mixing degree (ψ) at the different altitudes for P1 and P2.

$$\tan(\beta) = \frac{1 - r^3/r_0^3}{1 - n/n_0} \tag{1}$$

$$\psi = \frac{\beta}{\pi/2} \tag{2}$$

Here, r is the mvr for each hologram and the rest of the variables are the same as those used while generating the mixing diagrams. Average values of β and ψ are then obtained for the entire cloud segment at each altitude. The extreme homogeneous and inhomogeneous mixing processes correspond to $\psi = 1$ and $\psi = 0$, respectively. A larger value of ψ indicates a higher HM degree, negative values suggest that mvr is larger than the adiabatic value due to processes that can generate super-adiabatic drops such as IM&G and CC. According to table 1 cloud base shows a higher HM degree compared to cloud top which has a value closer to zero for both P1 and P2. The negative values of ψ at cloud middle level, suggest that mvr was larger than the adiabatic value for both P1 and P2 due to processes such as IM&G and CC. The ψ value for the CC case is significantly negative and indicates a strongly negative correlation between mvr and droplet number.

3.4 Analysis of dynamical measures

In order to understand why we observe the vertical variation of homogeneous mixing degree seen in the previous subsection, we must examine the relative magnitudes of local turbulence mixing and microphysical time scales which dictate the microphysical behavior of cloud droplets during an entrainment-mixing process (Baker et al., 1980). Here we evaluate two such common dynamical measures, Damköhler number (Da) and transition scale number (N_L). Da is defined as the ratio of the turbulent mixing time scale (τ_m) to the droplet microphysical time scale (τ_r) (Lehmann et al., 2009)

$$Da = \frac{\tau_m}{\tau_r} \tag{3}$$

If $Da << 1$, entrained air can mix faster than the droplets can react and HM occurs. If $Da >> 1$, the droplets react fast enough for some of them to completely evaporate and IM occurs. Here, we use the large eddy turnover time as the mixing time scale, cal-

culated using the following equation based on Kolmogorov scaling theory (Wyngaard, 2010):

$$\tau_m = \frac{u'^2}{\varepsilon} \tag{4}$$

and the large eddy length scale is estimated with:

$$l_e = \tau_m \times u' \tag{5}$$

where u' denotes the root mean square vertical velocity fluctuations and ε is the mean turbulence kinetic energy dissipation rate. We obtain ε by normalizing the obtained wind velocity structure functions (S_u) by the scaled spatial lag $r^{2/3}$ predicted by Kolmogorov theory (Wyngaard, 2010).

$$S_u = [u'(x) - u'(x+r)]^2 \tag{6}$$

$$\varepsilon = \left[\frac{S_u}{2r^{2/3}}\right]^{3/2} \tag{7}$$

Here, we use wind velocities for the same 1-2 minute cloud segments coincident with HOLODEC data. Thus the local air turbulence properties in the vicinity of the droplets are considered instead of an average value for the entire horizontal flight leg. The resulting plateau value provides a good estimate of local ε (Desai et al., 2019). It is worth noting that the velocity auto-correlation time scale has been used by others as τ_m as well. However, for our measurements, a 20 Hz wind velocity signal is obtained using the AIMMS-20 probe on board the aircraft. For a mean flight speed of 100 m s^{-1}, this gives a spatial resolution of 5 m. This spatial resolution is too coarse to allow accurate characterization of the velocity auto-correlation time scale for this study.

Multiple time scales have been used to represent the droplet microphysical time scale (τ_r) and has lead to considerable disagreements within the cloud community (Lu et al., 2018). One such commonly used microphysical time scale is the phase relaxation time scale (τ_c), defined as (Cooper, 1989):

$$\tau_c = \frac{1}{4\pi D n \overline{r}} \tag{8}$$

where, D is the modified water vapor diffusion coefficient to include thermal effects (Rogers & Yau, 1989) and $n\overline{r}$ is the integral radius (Cooper, 1989; Desai et al., 2018). Another commonly used microphysical time scale is the droplet evaporation time (τ_e), defined as (Lu et al., 2018):

$$\tau_e = -\frac{r_a^2}{2AS_0} \tag{9}$$

where, r_a is the adiabatic droplet radius, taken here as the mvr, A is the growth parameter and S_0 is the saturation deficit of entrained dry air. We assume that the initial decrease in RH above cloud top happens within the entrainment interfacial layer (Katzwinkel et al., 2012) and sudden decrease in T_{dp} signals cloud top clear air. The cloud top dry air $S_0 = 45\%$ ($RH = 55\%$) is determined from the vertical soundings (fig. 2).

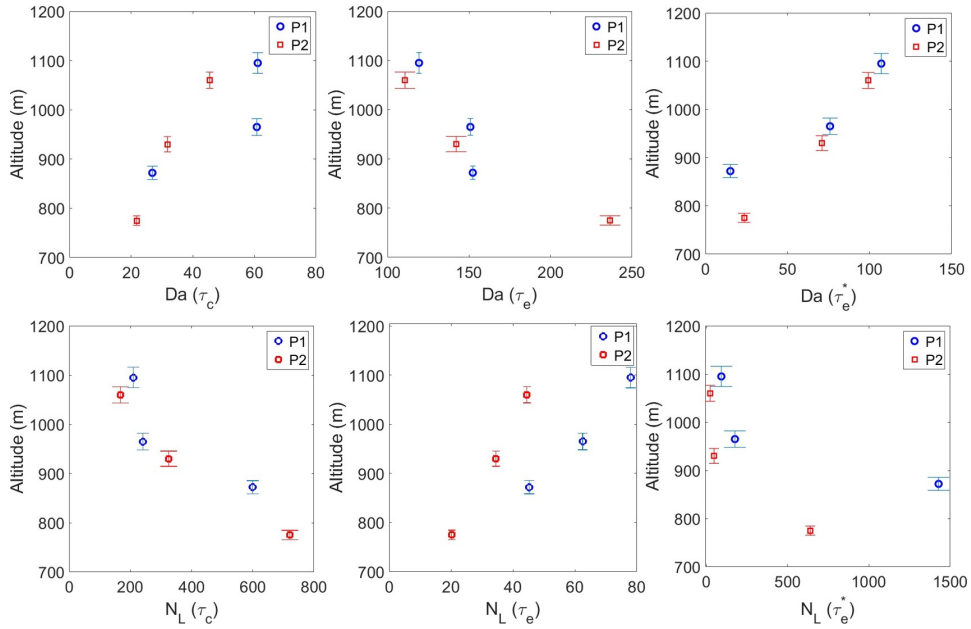

Figure 5. The top row shows Da and the bottom row shows N_L calculated using τ_c (left), τ_e (middle) and τ_e* (right) respectively as the droplet reaction time scale, with respect to altitude. P1 points are in blue while P2 points are in red.

Another dynamical measure for studying the mixing type is the transition scale number (N_L) defined as (Lu et al., 2011; Yeom et al., 2017):

$$N_L = \frac{L^*}{\eta} \tag{10}$$

where,

$$L^* = \varepsilon^{1/2}\tau_r^{3/2} \tag{11}$$

is the transition length scale defined as the turbulent eddy size at $Da = 1$ (Lehmann et al., 2009) and,

$$\eta = \left(\frac{\nu^3}{\varepsilon}\right)^{1/4} \tag{12}$$

is the Kolmogorov length scale, with ν being the kinematic viscosity.

Due to the disagreements in the cloud community, here we examine both microphysical timescales and attempt to determine which of them is able to correctly predict the entrainment-mixing behavior observed using HOLODEC and which corresponding parameter used by the two timescales, dominates the response of the droplets. Fig. 5 shows the vertical profiles of Da (top row) and N_L (bottom row) calculated using τ_c (left) and τ_e (middle) as the microphysical time scale respectively. It is interesting to see that Da calculated using τ_c increases with increasing altitude. This indicates that τ_m is considerably larger than τ_c near cloud top leading to IM. The two time scales are closer in magnitude to each other near cloud base leading to more HM (table 2). N_L calculated using τ_c as the microphysical time scale (bottom left) shows a decreasing trend with increasing altitude. This again indicates more IM near cloud top compared to HM near

cloud base. These trends for Da and N_L agree well with each other and are consistent with the observed microphysical behavior shown using mixing diagrams in fig. 4. However, the change with altitude for Da and N_L calculated with τ_e as the microphysical time scale suggests more HM near cloud top and IM near cloud base which seems contradictory to the mixing diagram results and HM degree.

4 A new model for vertical variation of saturation deficit

The contrast between using phase relaxation and evaporation time scales in calculation of Da and N_L agrees well with DNS results by Z. Gao et al. (2018) and is worth highlighting. In particular, the results using evaporation time scale appears at odds with the homogeneous mixing degree and the recommendation of Lu et al. (2018) and Z. Gao et al. (2018) to use evaporation time scale in investigation of entrainment-mixing processes. This contradiction suggests a need for a deeper examination of the droplet microphysical time scales in order to better understand the small scale entrainment-mixing processes occurring in these clouds.

Both τ_m and τ_c are calculated using local turbulence measurements and local microphysical measurements respectively at each altitude. Note that τ_e (eq. 9) takes into account local mean droplet radius, but assumes that S_0 is constant across multiple altitudes. This assumption has been commonly used in previous studies (Yeom et al., 2017; Lu et al., 2018). For our measurements of stratocumulus clouds, where entrainment primarily occurs at cloud top (Wood, 2012), cloud top radiative and evaporative cooling results in some negatively buoyant entrained parcels descending through the cloud (J. Wang et al., 2009; Yum et al., 2015). However, if the rate of descent is slower than the average mixing time scale, this parcel will mix with surrounding cloudy air and approach saturation by the time it reaches the cloud base. For the data presented in this paper, the average cloud height for P1 and P2 was about 250 m and rms vertical velocity was 0.5 m s^{-1}. This suggests that a descending parcel should require at least 500 s to descend from cloud top to cloud base. Given average turbulent mixing time scale $\overline{\tau_m} = 230$ s (table 2), we can assume that the descending parcel is well mixed by the time it reached cloud base. Thus S_0 should not be a constant, but decrease as a function of distance traveled by the descending parcel. If we assume a linear mixing behavior, the parcel water vapor mixing ratio can be expressed as:

$$q_v(z) = q_{v,0} + \frac{z}{H}[q_{v,s}(z) - q_{v,0}] \tag{13}$$

and,

$$S_0(z) = \frac{q_v(z)}{q_{v,s}(z)} - 1 \tag{14}$$

where, $q_{v,0}$ is the water vapor mixing ratio of the entrained dry air above cloud, $q_{v,s}$ is the saturated water vapor mixing ratio, H is the cloud thickness and z is the distance travelled by the descending parcel through the cloud (positive downwards). Thus, at $z = 0$, or cloud top, $q_v(0) = q_{v,0}$ and at $z = H$, $q_v(H) = q_{v,s}$. For our calculations, we use $z = 0.1H$ and $0.9H$ at cloud top and cloud base respectively to account for the flight level not being level with cloud top/base and to avoid $S_0 = 0$ in the denominator. Using these new values, we obtain a height dependent saturation deficit S_0^*, a corresponding height dependent evaporation time τ_e^* and recalculate Da and N_L using them.

Fig. 5 shows the recalculated vertical profiles of Da (top right) and N_L (bottom right) using the modified τ_e^* as the droplet microphysical time scale. We see that Da now increases with increasing altitude while N_L steadily decreases with increasing altitude. Both profiles now suggest more IM near cloud top compared to more HM near cloud base,

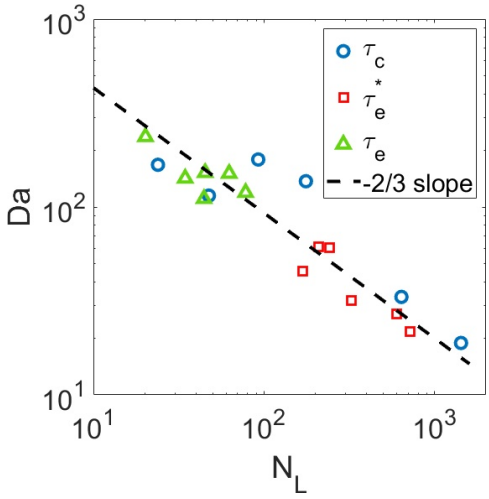

Figure 6. *Da* values obtained using different microphysical time scales as a function of N_L show a consistent negative two-thirds slope on a logarithmic scale.

consistent with the mixing diagram observations and the Da, N_L trends calculated using τ_c as the microphysical time scale (table 2). The result suggests that it is critical to use accurate S_0 values while calculating τ_e especially where significant variation of S_0 is expected.

5 Further discussion

The above analysis raises two questions meriting further discussion. First, why is the modified evaporation time and the phase relaxation time more appropriate to study the vertical variation of entrainment-mixing processes compared to the conventional droplet evaporation time? Since τ_c (eq. 8) does not consider the time required to completely evaporate an individual droplet, Lu et al. (2018) argued that the τ_e is relevant microphysical timescale for mixing events which involve complete droplet evaporation. They also suggest that τ_c is more suitable for non-complete evaporation phenomenon such as droplet condensational growth due to supersaturation fluctuations (Desai et al., 2018). While that is a sound argument, Srivastava (1989) argues that droplet evaporation rate during entrainment-mixing events will be influenced by the local supersaturation which in turn will be determined by the local droplet population (Cooper, 1989). Thus, τ_c which does consider the local droplet number concentration may still be a relevant time scale for mixing as shown by Pinsky et al. (2016). τ_e on the other hand, does not consider the local droplet number concentration, but considers each droplet as an individual droplet reacting to entrained air. It also assumes the saturation deficit to be constant, which can only be true for fast mixing processes. This paper shows that the effect of variability in S_0 is an important consideration when calculating τ_e for marine stratocumulus clouds where mixing time scales can be quite large (Wyngaard, 2010). Lehmann et al. (2009) argued that the effective droplet reaction time scale must be a combination of τ_c and τ_e with the smaller timescale dominating the effect. A system timescale approach similar to Chandrakar et al. (2016) also suggests more HM near cloud top and IM near cloud base since it is influenced strongly by the smaller timescale, which in this case is τ_e (SI). Lu et al. (2018) also argued that τ_c and τ_e will be equivalent to each other if the ratio of LWC to S_0 remains constant. However, in our case LWC increases with height within the stratocumulus layer (table 1) and a constant S_0 will cause the ratio to increase as

Level	ε	τ_m	τ_c	τ_e	τ_e^*	$Da(\tau_e)$	$Da(\tau_e^*)$	$N_L(\tau_e)$	$N_L(\tau_e^*)$
P1 Base	$1.7e^{-3}$	175.1	6.51	1.16	11.6	152.3	15.2	45.2	1428
Mid	$1.4e^{-3}$	241.3	3.89	1.59	3.18	150.8	75.9	62.5	176
Top	$1.3e^{-3}$	229.1	3.74	1.92	2.14	119.3	107	78.0	92.5
P2 Base	$7.5e^{-4}$	253.1	11.6	1.07	10.7	236.5	23.6	20.2	639
Mid	$5.9e^{-4}$	241.6	7.59	1.70	3.40	142.2	71.0	34.5	47.5
Top	$5.4e^{-4}$	238.3	5.23	2.15	2.38	110.7	99.2	44.5	23.9

Table 2. Turbulence measurements at three altitudes for P1 and P2: turbulence kinetic energy dissipation rate (ε) in m^2s^{-3}, mixing time scale (τ_m) in s, phase relaxation time (τ_c) in s, droplet evaporation time (τ_e), modified evaporation time scale (τ_e^*), Damköhler numbers calculated using τ_e and τ_e^* and transition scale numbers using τ_e and τ_e^*.

well. Considering vertical variation of S_0 with height (eq. 13) allows the ratio of LWC to S_0 to remain fairly steady and τ_e^* to be more comparable to τ_c (fig. 7).

Secondly, the use of Da and N_L yields qualitatively consistent conclusions on the vertical variation of entrainment-mixing processes which suggests a negative correlation between the two dimensionless numbers (fig. 6). Reorganization of their definition equations leads to:

$$Da = \frac{u'^2}{(\varepsilon\nu)^{1/2}} N_L^{-2/3} \tag{15}$$

which confirms the negative correlation provided the dimensionless pre-factor is constant. In our calculations, the pre-factor value remains fairly constant between 2085-2255, which is a small range considering the two orders of magnitude variation in Da and N_L (fig. 6). This agrees with Z. Gao et al. (2018) who showed a negative correlation between Da and N_L using DNS. Eq. 15 also indicates that the dimensionless pre-factor is a ratio of the turbulent kinetic energy to the energy in the Kolmogorov dissipation scale. It reiterates the interaction occurring during mixing between different scales, similar to the turbulence energy cascade.

Da compares the large scale turbulent mixing time (τ_m) with the microphysical time scale to explain the mixing behavior. While the exact values of τ_m may seem orders of magnitude larger than the droplet microphysical time scales, it may be due to the coarse spatial resolution for wind velocity fluctuation measurements. Thus, we focus on the relative trend with altitude and the relative behavior of the two timescales with respect to height. Table 2 indicates that the value of τ_m does not vary linearly with altitude. But τ_c shows a monotonic decrease with altitude. This is because τ_c is inversely proportional to the droplet integral radius (eq. 8) and an increase in integral radius with altitude results in τ_c being considerably smaller near cloud top compared to cloud base (fig. 7). The interplay of τ_m and τ_c with altitude results in an increase in Da with increasing altitude, leading to HM near cloud base and IM near cloud top. Thus Da and N_L calculations using τ_c also indicate IM near cloud top and HM near cloud base.

On the other hand, τ_e increases with height, contrary to τ_c, as can be seen in fig. 7. This would suggest that the droplet microphysical time is larger at cloud top leading to a slower response to entrainment-mixing compared to cloud base. This is counter intuitive since cloud top droplets are the first ones to interact with a dry entrained parcel compared to cloud base droplets. Thus, to account for the variation of S_0 due to droplet

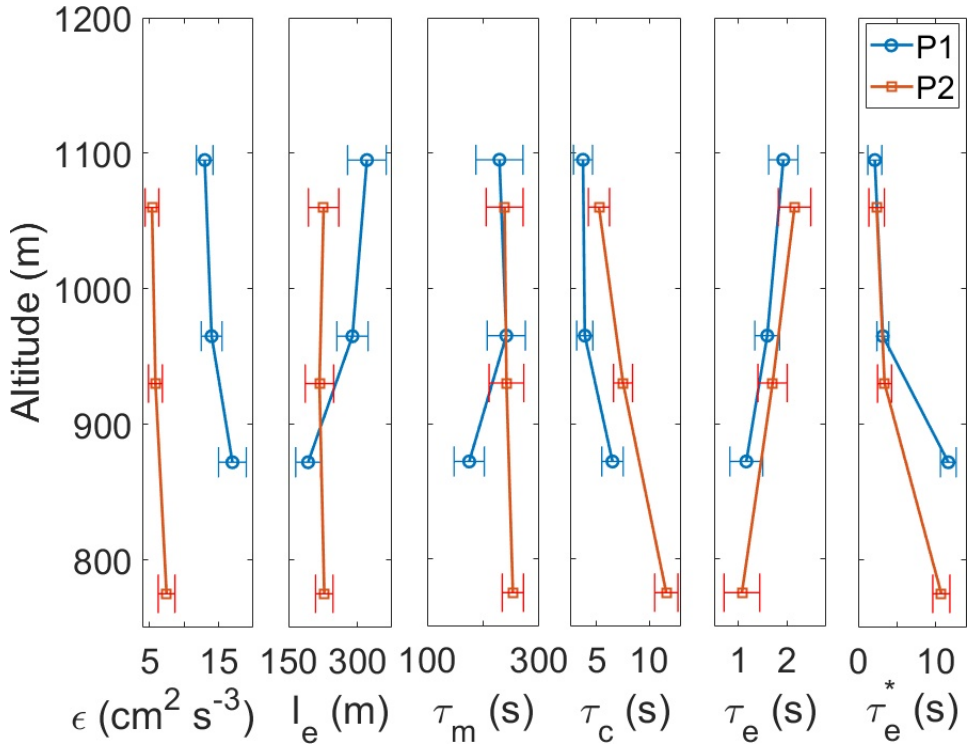

Figure 7. (Left to right) TKE dissipation rate (ε), large eddy length scale (l_e), mixing time scale (τ_m), phase relaxation time scale (τ_c), droplet evaporation time scale (τ_e) and the modified evaporation time scale (τ_e^*) with respect to altitude. P1 points are in blue while P2 points are in red.

evaporation as mixing proceeds from cloud top towards cloud base for stratocumulus clouds, we propose a simple linear mixing model (eq. 13). The modified values of τ_e can now be seen to decrease with height within the cloud which is consistent with τ_c (fig. 7). The modified Da now provides a more consistent picture of the mixing behavior with mixing diagrams, homogeneous mixing degree and τ_c.

This analysis shines a new light on the usage of τ_c or τ_e as the droplet microphysical time scale. τ_c considers the local droplet environment due to droplet number concentration whereas τ_e considers droplet size and local saturation deficit. For the current dataset, both droplet number concentration and saturation deficit increase with height, resulting in smaller microphysical timescales with increasing altitude. Whereas, droplet radius which also increases with altitude suggests larger microphysical timescales with increasing altitude for τ_e which considers each droplet behaving individually. The combination of these factors result in the mixing behavior as shown by the mixing diagrams. It is entirely possible that for another dataset, the environmental and microphysical conditions will result in a different combination of factors dominating the mixing behavior and the time scales which represent those factors will be better at representing the mixing behavior. Thus it is important to examine each of these factors and use the respective time scale to understand mixing type.

6 Summary

Marine stratocumulus clouds cover vast portions of the Earth's surface and contribute significantly to the net radiative budget. While their extent can be measured in

hundreds or thousands of kilometers, sub-grid scale variability in albedo can cause large uncertainties in climate models attempting to represent them (Bony & Dufresne, 2005; Dal Gesso et al., 2015). These variabilities are caused by sub-meter scale processes that determine entrainment rate, cloud lifetime and precipitation rate (Mellado, 2017). Yum et al. (2015) predicted that mixing might be inhomogeneous near cloud top and progressively becomes homogeneous near cloud base. However, high resolution measurements at multiple altitudes within a stratocumulus deck have been rare (Wood, 2005) and available measurements are plagued by spatial averaging. In this paper, we analyze airborne measurements taken at multiple altitudes within a stratocumulus cloud layer during the ACE-ENA campaign using HOLODEC. HOLODEC is unique in its sampling since every hologram provides a centimeter scale measurement of droplet number and size avoiding the effects of spatial averaging across meter scale regions which may be affected by varying degrees of mixing.

Results indicate a monotonic increase in cloud droplet properties such as droplet mean volume radius and LWC with height within the cloud layer. Entrainment mixing likely plays a significant role in establishing such a gradient within stratocumulus clouds. Mixing is shown to be inhomogeneous near cloud top and homogeneous near cloud base based on mixing diagram analysis and homogeneous mixing degree calculations. Turbulence and cloud microphysical measurements indicate that droplet microphysical timescale decreases with increasing altitude within the cloud while the mixing time scale stays relatively constant. This behavior of the two timescales allows cloud top droplets to quickly evaporate due to entrainment while those at cloud base react comparatively slowly. IM near cloud top, facilitates growth of the remaining droplets through condensation due to a reduction in droplet number concentration and increasing the supersaturation fluctuations. HM near cloud base results in reduction in mean droplet size. This gradient in droplet size in the vertical direction allows larger droplets at higher altitudes to fall through the lower layers and collect smaller droplets along the way, promoting collision-coalescence and drizzle formation. Evidence of such processes may be seen in the cloud middle layers.

There has been some debate in the cloud community regarding which microphysical timescale should be considered while studying entrainment-mixing processes. In this paper, we examined the phase relaxation and droplet evaporation timescales as possible candidates. The results show that the phase relaxation time provides a consistent picture of mixing type variation with altitude, while the conventional evaporation time does not. This is because droplet evaporation time definition does not consider local saturation deficit. We believe that local saturation deficit should decrease from cloud top towards clouds base due to droplet evaporation and mixing. We proposed a modification of the evaporation time equation to account for this variation leading to better agreement with mixing type variation with height. Two points are noteworthy: first, the study ignores possible secondary activation of cloud droplets occurring near cloud top due to entrainment of free tropospheric air and aerosol particles (J. Chen et al., 2020). If secondary activation does occur, we expect the newly formed droplets to be smaller than the lower detection limit of HOLODEC. As such, the effect of secondary activation on cloud properties merits further investigation for the data used in this paper. A related topic is to quantify the effect of aerosol size distributions on this type of entrainment-mixing and drizzle formation and in turn the effect of mixing and drizzle on the aerosol size distribution. Secondly, this study represents a single research flight during the campaign and does not suggest that the same microphysical behavior should persist in marine stratocumulus clouds for every day of the year. While the entrainment-mixing and drizzling behavior observed here is quite representative of our understanding of marine stratocumulus clouds (Wood, 2005; J. Wang et al., 2009; Yum et al., 2015), certain environmental perturbations such as cold fronts (kazemirad & Miller, 2020) and increased aerosol loading (Zheng et al., 2020) can affect cloud microphysics significantly. Further studies involving all available research flights during multiple such IOPs to include sea-

sonal variations should provide a better understanding of microphysical variability in marine stratocumulus clouds.

Acknowledgments

This research was supported by the U.S. Department of Energy Atmospheric System Research (ASR) program (DESC00112704) and Solar Energy Technologies Office (SETO) under Award 33504. R. Shaw's participation was supported by the U.S. Department of Energy Atmospheric System Research (ASR) program (DESC0020053). C. Lu and S. Gao's participation was supported by the National Natural Science Foundation of China (41822504). Superior, a high-performance computing infrastructure at Michigan Technological University, and the supercomputer MOGON and/or advisory services offered by Johannes Gutenberg University Mainz (hpc.uni-mainz.de), were used in reconstructing holographic results. We also acknowledge the support of the HoloSuite software team for their contributions to the hologram processing software. The ACE-ENA campaign was supported by the Atmospheric Radiation Measurement (ARM) user facility, a U.S. Department of Energy (DOE) office of science user facility managed by the Biological and Environmental Research Program. We thank Alyssa Mathews at PNNL, and the entire G-1 aircraft and field campaign team. The ACE-ENA data is available "`https://www.arm.gov/research/campaigns/aaf2017ace-ena`".

References

Andrejczuk, M., Grabowski, W. W., Malinowski, S. P., & Smolarkiewicz, P. K. (2006). Numerical simulation of cloud–clear air interfacial mixing: Effects on cloud microphysics. *Journal of the atmospheric sciences*, *63*(12), 3204–3225.

Baker, M., Corbin, R., & Latham, J. (1980). The influence of entrainment on the evolution of cloud droplet spectra: I. a model of inhomogeneous mixing. *Quarterly Journal of the Royal Meteorological Society*, *106*(449), 581–598.

Beals, M. J., Fugal, J. P., Shaw, R. A., Lu, J., Spuler, S. M., & Stith, J. L. (2015). Holographic measurements of inhomogeneous cloud mixing at the centimeter scale. *Science*, *350*, 87–90.

Bony, S., & Dufresne, J.-L. (2005). Marine boundary layer clouds at the heart of tropical cloud feedback uncertainties in climate models. *Geophysical Research Letters*, *32*(20).

Brenguier, J.-L., & Grabowski, W. W. (1993). Cumulus entrainment and cloud droplet spectra: A numerical model within a two-dimensional dynamical framework. *Journal of the atmospheric sciences*, *50*(1), 120–136.

Burnet, F., & Brenguier, J.-L. (2007). Observational study of the entrainment-mixing process in warm convective clouds. *Journal of the atmospheric sciences*, *64*(6), 1995–2011.

Chandrakar, K. K., Cantrell, W., Chang, K., Ciochetto, D., Niedermeier, D., Ovchinnikov, M., ... Yang, F. (2016). Aerosol indirect effect from turbulence-induced broadening of cloud-droplet size distributions. *Proceedings of the National Academy of Sciences*, *113*(50), 14243–14248.

Chen, J., Liu, Y., & Zhang, M. (2020). Effects of lateral entrainment-mixing with entrained aerosols on cloud microphysics. *Geophysical Research Letters*, e2020GL087667.

Chen, S., Yau, M., & Bartello, P. (2018). Turbulence effects of collision efficiency and broadening of droplet size distribution in cumulus clouds. *Journal of the Atmospheric Sciences*, *75*(1), 203–217.

Chen, S., Yau, M.-K., Bartello, P., & Xue, L. (2018). Bridging the condensation–collision size gap: a direct numerical simulation of continuous droplet growth in turbulent clouds. *Atmospheric Chemistry and Physics*, *18*(10), 7251–7262.

Cooper, W. A. (1989). Effects of variable droplet growth histories on droplet size

distributions. Part I: Theory. *J. Atmos. Sci.*, *46*, 1301–1311.

Cooper, W. A., Lasher-Trapp, S. G., & Blyth, A. M. (2013). The influence of entrainment and mixing on the initial formation of rain in a warm cumulus cloud. *Journal of the Atmospheric Sciences*, *70*(6), 1727–1743.

Dal Gesso, S., Van der Dussen, J., Siebesma, A., De Roode, S., Boutle, I., Kamae, Y., ... Vial, J. (2015). A single-column model intercomparison on the stratocumulus representation in present-day and future climate. *Journal of Advances in Modeling Earth Systems*, *7*(2), 617–647.

Desai, N., Chandrakar, K., Chang, K., Cantrell, W., & Shaw, R. (2018). Influence of microphysical variability on stochastic condensation in a turbulent laboratory cloud. *Journal of the Atmospheric Sciences*, *75*(1), 189–201.

Desai, N., Glienke, S., Fugal, J., & Shaw, R. (2019). Search for microphysical signatures of stochastic condensation in marine boundary layer clouds using airborne digital holography. *Journal of Geophysical Research: Atmospheres*, *124*(5), 2739–2752.

Duda, D. P., Stephens, G. L., & Cox, S. (1991). Microphysical and radiative properties of marine stratocumulus from tethered balloon measurements. *Journal of Applied Meteorology*, *30*(2), 170–186.

Duynkerke, P. G., Zhang, H. Q., & Jonker, P. J. (1995). Microphysical and turbulent structure of nocturnal stratocumulus as observed during astex. *Journal of the atmospheric sciences*, *52*(16), 2763–2777.

Eastman, R., Warren, S. G., & Hahn, C. J. (2011). Variations in cloud cover and cloud types over the ocean from surface observations, 1954–2008. *Journal of Climate*, *24*(22), 5914–5934.

Fisher, R. A. (2006). *Statistical methods for research workers*. Genesis Publishing Pvt Ltd.

Fugal, J., & Shaw, R. (2009). Cloud particle size distributions measured with an airborne digital in-line holographic instrument. *Atmospheric Measurement Techniques*, *2*(1), 259–271.

Fugal, J. P., Schulz, T. J., & Shaw, R. A. (2009). Practical methods for automated reconstruction and characterization of particles in digital in-line holograms. *Measurement Science and Technology*, *20*(7), 075501.

Fugal, J. P., Shaw, R. A., Saw, E. W., & Sergeyev, A. V. (2004). Airborne digital holographic system for cloud particle measurements. *Appl. Opt.*, *43*, 5987–5995.

Gao, S., Lu, C., Liu, Y., Mei, F., Wang, J., Zhu, L., & Yan, S. (2020). Contrasting scale dependence of entrainment-mixing mechanisms in stratocumulus clouds. *Geophysical Research Letters*, *47*(9), e2020GL086970.

Gao, Z., Liu, Y., Li, X., & Lu, C. (2018). Investigation of turbulent entrainment-mixing processes with a new particle-resolved direct numerical simulation model. *Journal of Geophysical Research: Atmospheres*, *123*(4), 2194–2214.

Ghate, V. P., & Cadeddu, M. P. (2019). Drizzle and turbulence below closed cellular marine stratocumulus clouds. *Journal of Geophysical Research: Atmospheres*, *124*(11), 5724–5737.

Giangrande, S. E., Wang, D., Bartholomew, M. J., Jensen, M. P., Mechem, D. B., Hardin, J. C., & Wood, R. (2019). Midlatitude oceanic cloud and precipitation properties as sampled by the arm eastern north atlantic observatory. *Journal of Geophysical Research: Atmospheres*, *124*(8), 4741–4760.

Glassmeier, F., & Feingold, G. (2017). Network approach to patterns in stratocumulus clouds. *Proceedings of the National Academy of Sciences*, *114*(40), 10578–10583.

Goren, T., & Rosenfeld, D. (2015). Extensive closed cell marine stratocumulus downwind of europea large aerosol cloud mediated radiative effect or forcing? *Journal of Geophysical Research: Atmospheres*, *120*(12), 6098–6116.

Grabowski, W. W., & Wang, L.-P. (2013). Growth of cloud droplets in a turbulent

environment. *Annual review of fluid mechanics*, *45*, 293–324.

Henneberger, J. F.-W. (2013). *Mountain-top in-situ observations of mixed-phase clouds with a digital holographic instrument* (Doctoral dissertation, ETH Zurich). doi: 10.3929/ethz-a-010088759

Hill, A. A., Feingold, G., & Jiang, H. (2009). The influence of entrainment and mixing assumption on aerosol–cloud interactions in marine stratocumulus. *Journal of the Atmospheric Sciences*, *66*(5), 1450–1464.

Hoffmann, F., & Feingold, G. (2019). Entrainment and mixing in stratocumulus: Effects of a new explicit subgrid-scale scheme for large-eddy simulations with particle-based microphysics. *Journal of the Atmospheric Sciences*, *76*(7), 1955–1973.

Hudson, J. G., & Yum, S. S. (1997). Droplet spectral broadening in marine stratus. *Journal of the atmospheric sciences*, *54*(22), 2642–2654.

Katzwinkel, J., Siebert, H., & Shaw, R. (2012). Observation of a self-limiting, shear-induced turbulent inversion layer above marine stratocumulus. *Boundary-layer meteorology*, *145*(1), 131–143.

kazemirad, M., & Miller, M. A. (2020). Summertime post-cold-frontal marine stratocumulus transition processes over the eastern north atlantic. *Journal of the Atmospheric Sciences*, *77*(6), 2011–2037.

Lasher-trapp, S. G., Cooper, W. A., & Blyth, A. M. (2005). Broadening of droplet size distributions from entrainment and mixing in a cumulus cloud. *Quarterly Journal of the Royal Meteorological Society: A journal of the atmospheric sciences, applied meteorology and physical oceanography*, *131*(605), 195–220.

Lehmann, K., Siebert, H., & Shaw, R. A. (2009). Homogeneous and inhomogeneous mixing in cumulus clouds: Dependence on local turbulence structure. *Journal of the Atmospheric Sciences*, *66*(12), 3641–3659.

Liu, Y., & Daum, P. H. (2000). Spectral dispersion of cloud droplet size distributions and the parameterization of cloud droplet effective radius. *Geophysical research letters*, *27*(13), 1903–1906.

Liu, Y., Daum, P. H., McGraw, R. L., Miller, M. A., & Niu, S. (2007). Theoretical expression for the autoconversion rate of the cloud droplet number concentration. *Geophysical research letters*, *34*(16).

Liu, Y., & Hallett, J. (1998). On size distributions of cloud droplets growing by condensation: A new conceptual model. *Journal of the atmospheric sciences*, *55*(4), 527–536.

Lu, C., Liu, Y., & Niu, S. (2011). Examination of turbulent entrainment-mixing mechanisms using a combined approach. *Journal of Geophysical Research: Atmospheres*, *116*(D20).

Lu, C., Liu, Y., Niu, S., & Endo, S. (2014). Scale dependence of entrainment-mixing mechanisms in cumulus clouds. *Journal of Geophysical Research: Atmospheres*, *119*(24), 13–877.

Lu, C., Liu, Y., Zhu, B., Yum, S. S., Krueger, S. K., Qiu, Y., ... Luo, S. (2018). On which microphysical time scales to use in studies of entrainment-mixing mechanisms in clouds. *Journal of Geophysical Research: Atmospheres*, *123*(7), 3740–3756.

Lu, C., Niu, S., Liu, Y., & Vogelmann, A. M. (2013). Empirical relationship between entrainment rate and microphysics in cumulus clouds. *Geophysical Research Letters*, *40*(10), 2333–2338.

Magaritz-Ronen, L., Pinsky, M., & Khain, A. (2016). Drizzle formation in stratocumulus clouds: effects of turbulent mixing. *Atmospheric Chemistry and Physics (Online)*, *16*(3).

Mellado, J. P. (2017). Cloud-top entrainment in stratocumulus clouds. *Annual Review of Fluid Mechanics*, *49*, 145–169.

Paluch, I. R., & Knight, C. A. (1984). Mixing and the evolution of cloud droplet size spectra in a vigorous continental cumulus. *Journal of the atmospheric sciences*,

41(11), 1801–1815.

Paoli, R., & Shariff, K. (2009). Turbulent condensation of droplets: Direct simulation and a stochastic model. *Journal of the atmospheric sciences*, *66*(3), 723–740.

Pawlowska, H., & Brenguier, J.-L. (2000). Microphysical properties of stratocumulus clouds during ace-2. *Tellus B*, *52*(2), 868–887.

Pinsky, M., Khain, A., & Korolev, A. (2016). Theoretical analysis of mixing in liquid clouds–part 3: Inhomogeneous mixing. *Atmospheric Chemistry and Physics (Online)*, *16*(14).

Rogers, R., & Yau, M. (1989). *A short course in cloud physics*. Butterworth-Heinemann.

Sardina, G., Picano, F., Brandt, L., & Caballero, R. (2015). Continuous growth of droplet size variance due to condensation in turbulent clouds. *Phys. Rev. Lett.*, *115*, 184501.

Shaw, R. A. (2003). Particle-turbulence interactions in atmospheric clouds. *Ann. Rev. Fluid Mech.*, *35*, 183–227.

Spuler, S. M., & Fugal, J. (2011). Design of an in-line, digital holographic imaging system for airborne measurement of clouds. *Applied optics*, *50*(10), 1405–1412.

Srivastava, R. (1989). Growth of cloud drops by condensation: A criticism of currently accepted theory and a new approach. *Journal of the atmospheric sciences*, *46*(7), 869–887.

Stephens, G. L., & Greenwald, T. J. (1991). The earth's radiation budget and its relation to atmospheric hydrology: 2. observations of cloud effects. *Journal of Geophysical Research: Atmospheres*, *96*(D8), 15325–15340.

Telford, J. W., & Chai, S. K. (1980). A new aspect of condensation theory. *pure and applied geophysics*, *118*(2), 720–742.

Wang, J., Daum, P. H., Yum, S. S., Liu, Y., Senum, G. I., Lu, M.-L., ... Jonsson, H. (2009). Observations of marine stratocumulus microphysics and implications for processes controlling droplet spectra: Results from the marine stratus/stratocumulus experiment. *Journal of Geophysical Research: Atmospheres*, *114*(D18).

Wang, J., Wood, R., Jensen, M., Azevedo, E., Bretherton, C., Chand, D., ... others (2019). *Aerosol and cloud experiments in eastern north atlantic (ace-ena) field campaign report* (Tech. Rep.). DOE Office of Science Atmospheric Radiation Measurement (ARM) Program .

Wang, L.-P., & Grabowski, W. W. (2009). The role of air turbulence in warm rain initiation. *Atmospheric Science Letters*, *10*(1), 1–8.

Warner, J. (1973). The microstructure of cumulus cloud: Part iv. the effect on the droplet spectrum of mixing between cloud and environment. *Journal of the Atmospheric Sciences*, *30*(2), 256–261.

Warren, S. G., Eastman, R. M., & Hahn, C. J. (2007). A survey of changes in cloud cover and cloud types over land from surface observations, 1971–96. *Journal of climate*, *20*(4), 717–738.

Woittiez, E. J., Jonker, H. J., & Portela, L. M. (2009). On the combined effects of turbulence and gravity on droplet collisions in clouds: a numerical study. *Journal of the atmospheric sciences*, *66*(7), 1926–1943.

Wood, R. (2005). Drizzle in stratiform boundary layer clouds. part i: Vertical and horizontal structure. *Journal of the Atmospheric Sciences*, *62*(9), 3011–3033.

Wood, R. (2012). Stratocumulus clouds. *Monthly Weather Review*, *140*(8), 2373–2423.

Wood, R., O, K.-T., Bretherton, C. S., Mohrmann, J., Albrecht, B. A., Zuidema, P., ... others (2018). Ultraclean layers and optically thin clouds in the stratocumulus-to-cumulus transition. part i: Observations. *Journal of the Atmospheric Sciences*, *75*(5), 1631–1652.

Wyngaard, J. C. (2010). *Turbulence in the atmosphere*. Cambridge University Press.

Xie, X., & Liu, X. (2009). Analytical three-moment autoconversion parameterization based on generalized gamma distribution. *Journal of Geophysical Research: Atmospheres*, *114*(D17).

Yang, F., McGraw, R., Luke, E. P., Zhang, D., Kollias, P., & Vogelmann, A. M. (2019). A new approach to estimate supersaturation fluctuations in stratocumulus cloud using ground-based remote-sensing measurements. *Atmospheric Measurement Techniques*, *12*(11), 5817–5828.

Yang, F., Shaw, R., & Xue, H. (2016). Conditions for super-adiabatic droplet growth after entrainment mixing. *Atmospheric Chemistry and Physics*, *16*(14), 9421.

Yeom, J. M., Yum, S. S., Liu, Y., & Lu, C. (2017). A study on the entrainment and mixing process in the continental stratocumulus clouds measured during the racoro campaign. *Atmospheric research*, *194*, 89–99.

Yum, S. S., & Hudson, J. G. (2001). Microphysical relationships in warm clouds. *Atmospheric research*, *57*(2), 81–104.

Yum, S. S., & Hudson, J. G. (2005). Adiabatic predictions and observations of cloud droplet spectral broadness. *Atmospheric research*, *73*(3-4), 203–223.

Yum, S. S., Wang, J., Liu, Y., Senum, G., Springston, S., McGraw, R., & Yeom, J. M. (2015). Cloud microphysical relationships and their implication on entrainment and mixing mechanism for the stratocumulus clouds measured during the vocals project. *Journal of Geophysical Research: Atmospheres*, *120*(10), 5047–5069.

Zhang, Z., Song, Q., Mechem, D., Larson, V., Wang, J., Liu, Y., ... Wu, P. (2020). Vertical dependence of horizontal variation of cloud microphysics: Observations from the ace-ena field campaign and implications for warm rain simulation in climate models. *Atmospheric Chemistry and Physics Discussions*, 1–46.

Zheng, G., Sedlacek, A. J., Aiken, A. C., Feng, Y., Watson, T. B., Raveh-Rubin, S., ... Wang, J. (2020). Long-range transported north american wildfire aerosols observed in marine boundary layer of eastern north atlantic. *Environment International*, *139*, 105680.